Parabolic versus spherical partial cross sections for photoionization excitation of He near threshold

C. Bouri,* P. Selles, and L. Malegat
LIXAM et Fédération LUMAT, CNRS et Université Paris-Sud 11, 91405 Orsay, France

M. G. Kwato Njock
CEPAMOQ, Faculty of Science, University of Douala, P.O. Box 8580, Douala, Cameroon
(Received 5 May 2006; published 18 September 2006)

Spherical and parabolic partial cross sections and asymmetry parameters, defined in the ejected electron frame, are presented for photoionization excitation of the helium atom at 0.1 eV above its double ionization threshold. A quantitative law giving the dominant spherical partial wave l_{dom} for each excitation level n is obtained. The parabolic partial cross sections are shown to satisfy the same approximate selection rules as the related Rydberg series of doubly excited states $(K,T)_n^A$. The analysis of radial and angular correlations reveals the close relationship between double excitation, ionization excitation, and double ionization. Opposite to a widespread belief, the observed value of the asymmetry parameter is shown to result from the interplay of radial correlations and symmetry constraints, irrespective of angular correlations. Finally, the measurement of parabolic partial cross sections is proposed as a challenge to experimentalists.

DOI: 10.1103/PhysRevA.74.032704 PACS number(s): 32.80.Fb

I. INTRODUCTION

It is widely acknowledged that one-photon double ionization of He would not occur in the absence of electronic correlations. The same holds for one-photon single ionization with excitation of the residual He^+ ion. Accordingly, the study of this one-photon two-electron process is expected to provide information on angular and radial correlations, complementary to that obtained from double ionization studies. This information is hidden in the integrated cross sections σ_n and asymmetry parameters β_n relevant to ionization with excitation to the level n of the residual hydrogenic ion. To extract it, one has to rewrite these quantities in terms of the contributions of the different partial waves of the bound electron. Here, we consider both spherical $[nlm]$ and parabolic $[n_1n_2m]$ partial waves defined with respect to the direction of the ejected electron.

Many authors indeed have been concerned with determining the relative weight of each spherical partial wave contribution σ_{nl} to a given cross section σ_n—be it a photon-impact ionization-excitation cross section or an electron-impact excitation cross section. Following the analysis of low-energy electron correlations by Wannier [1], Fano [2] was the first to emphasize that electron-impact on an atom close to its ionization threshold could populate high n and l Rydberg states. He conjectured that the highest l that could be populated significantly should vary as $\sqrt{n}$. Later on Drukarev [3] and Rau [4] predicted the angular momentum that dominates this process to be $l_{\mathrm{dom}}^D \simeq \sqrt{n/2}$ and $l_{\mathrm{dom}}^R \simeq \sqrt{n}/2$, respectively. These results were rederived later on [5], the additive factor $-1/2$ that had been discarded in the original papers being retained, leading to the introduction of $\tilde{l}_{\mathrm{dom}}^D \simeq \sqrt{n/2}-1/2$ and $\tilde{l}_{\mathrm{dom}}^R \simeq \sqrt{n}/2-1/2$. Some experimental evidence of the predicted laws has been obtained from threshold photoelectron spectra in the rare gases [5]. For hydrogenic systems, the Coulomb degeneracy of the l sublevels of a given n multiplet precludes the direct measurement of σ_{nl} by photoelectron spectroscopy. Estimates of σ_{2s} and σ_{2p} [6–8] as well as of σ_{3s}, σ_{3p}, and σ_{3d} in helium [7], roughly consistent with the theoretical predictions, have been obtained by analyzing the fluorescence decay of the excited ionic states. On the whole, the measurements are not accurate enough nor numerous enough to assess the validity of the predicted laws quantitatively. In this paper, we show that numerical simulations based on the method of the hyperspherical R-matrix method with semiclassical outgoing waves (HRM-SOW) offer a way out of the impasse.

Parabolic partial waves, on the other side, have been introduced historically in the study of the Stark effect in H (see Refs. [9,10], for instance). Later on, the group-theoretical analysis of doubly excited states by Herrick and co-workers made the new quantum numbers $[K,T]$ emerge [11–15]. Their relation to the parabolic quantum numbers of the inner electron with respect to the outer electron's direction, which reads $K=n_2-n_1$ and $T=|m|$, was recognized afterwards [16]. In between however, Drukarev [3] and Rau [4] had evaluated l_{dom} using the parabolic approach and the group-theoretical approach, respectively. The quasi-identity of their results was a first evidence of the close relationship between the quantum numbers introduced in these two approaches. In parallel, the adiabatic hyperspherical approach had led Lin [17,18] to introduce an additional quantum number A to characterize the behavior of doubly excited states in the exchange of the radial coordinates of the two electrons: $A=+1$ for symmetric states, $A=-1$ for antisymmetric ones, and $A=0$ in all other cases. As a result, the notation ${}_{n'}(KT)_n^A$ has established itself to name the successive members n' of Rydberg series of doubly excited states converging to the nth excitation threshold. Surprisingly, this classification scheme has never been applied to the continuum states to which these series con-

*Permanent address CEPAMOQ, Faculty of Science, University of Douala, P.O. Box 8580, Douala, Cameroon.

verge as $n' \to \infty$. In this paper, we fill this gap by analyzing ionization-excitation cross sections in terms of parabolic partial waves, thus demonstrating the continuity between double excitation and ionization excitation.

II. PARTIAL WAVE ANALYSIS

In a previous paper [19], we have presented cross sections σ_n and asymmetry parameters β_n for photoionization of He with excitation of the residual ion up to $n=50$. These data were obtained at only 0.1 eV above the double ionization threshold using the HRM-SOW method complemented by a fixed hyper-radius projection technique. Having this very complete set of data at our disposal gives us the opportunity to push the analysis in spherical partial waves one step further as well as to initiate an analysis in terms of parabolic partial waves.

A. Body-fixed expression of the photoabsorption wave function

A helium atom in its $^1S^e$ ground state, absorbing a single linearly polarized 79.1 eV photon, is promoted into a $^1P^o$ double continuum state. The latter is described by a two-electron wave function $\Psi(\vec{r}_1,\vec{r}_2)$, called the photoabsorption wave function, which is represented in our approach by the solution of a stationary inhomogeneous Schrödinger equation [25]. Using the hyper-radius $R=\sqrt{r_1^2+r_2^2}$, the hyperangle $\alpha=\arctan r_2/r_1$, and the collective notation Ω for the four spherical angles that specify the directions of the two electrons, this wave function reads

$$\Psi(R;\alpha,\Omega)=\sum_l \{f_l^+(R,\alpha)^+\mathcal{Y}_{ll+1}^{10}(\Omega)+f_l^-(R,\alpha)^-\mathcal{Y}_{ll+1}^{10}(\Omega)\}, \tag{1}$$

where the ${}^{\pm}\mathcal{Y}_{ll+1}^{10}$ are symmetrized $(+)$ and antisymmetrized $(-)$ normalized bipolar harmonics corresponding to a total angular momentum $L=1$ having a projection $M=0$ on the z axis of the laboratory frame (LF), the latter being taken along the polarization vector of the incident photon beam.

At the energy considered, photoabsorption promotes at least one electron into the continuum. Accordingly, we may define a body-fixed frame (BF) having its Z axis along the direction of an outgoing photoelectron, located by its spherical angles (θ,ϕ) in the LF. The X axis is chosen so that the direction of the other electron, which may be either bound or free, lies in the $X>0$ half of the XZ plane. This electron is located by the spherical angles $(\theta_{12},0)$ in the BF, where θ_{12} is the angle between the directions of the two electrons. The rotation that takes the LF into the BF is then characterized by the Euler angles (ϕ,θ,φ). The angle φ, which depends on the arbitrary orientation of the x axis of the LF, does not carry any relevant physical information and accordingly, it does not appear in the forthcoming expressions of the physical quantities. The first stage of our analysis consists in expressing the photoabsorption wave function $\Psi(R;\alpha,\Omega)$ in the BF. Applying the rotation $R(\phi,\theta,\varphi)$ on Eq. (1) and rearranging the resulting expression yields

$$\begin{aligned}\Psi(R;\alpha,\Omega)=\sum_{lm}(-1)^l Y_{1m}(\theta,\varphi)\Bigg\{&\frac{f_l^+(R,\alpha)+f_l^-(R,\alpha)}{\sqrt{2}}\\ &\times\langle l-m1m|l+10\rangle Y_{lm}(\theta_{12},0)\\ &-\frac{f_l^+(R,\alpha)-f_l^-(R,\alpha)}{\sqrt{2}}\\ &\times\langle l+1-m1m|l0\rangle Y_{l+1m}(\theta_{12},0)\Bigg\},\end{aligned} \tag{2}$$

where the $\langle l_1m_1l_2m_2|LM\rangle$ are Clebsh Gordan coefficients and the $Y_{lm}(\theta,\varphi)$ spherical harmonics.

This expression shows a remarkable simplicity. Indeed, due to the $^1P^o$ symmetry of the wave function and to the definition of the BF, the rotation matrix element involved reduces to the plain spherical harmonic $Y_{1m}(\theta,\varphi)$. It is then readily apparent that the projection of one electron's angular momentum on the photo electron's direction can only take three values, namely, $m=0,\pm1$. Moreover, if this projection is $m=0$, the angular distribution of the photoelectron is proportional to $\cos^2\theta$, the associated asymmetry parameter taking its maximum value $\beta=+2$, meaning that this electron travels preferentially along the direction of the electric field. Conversely, if this projection is $m=\pm1$, the angular distribution of the photoelectron is proportional to $\sin^2\theta$, the associated asymmetry parameter taking its minimum value $\beta=-1$, meaning that this electron travels preferentially perpendicular to the direction of the electric field. Note that this one-to-one correspondence between the asymmetry parameter and $T=|m|$ has already been emphasized by Greene [20].

B. Body-fixed expression of the ionization-excitation wave functions

The second stage of our analysis consists in projecting Ψ on the subspace spanned by all states in which one electron is in a specific bound state, characterized by a given set of quantum numbers defined with respect to the BF. As announced in the Introduction, we consider two different such sets, of which the first one is the spherical set $[nlm]$, while the second one is related to the parabolic quantum numbers $[n_1n_2m]$. These numbers satisfy $n=n_1+n_2+|m|+1$ as well as $K=n_2-n_1$, as noted above, so that the triplet $[n_1n_2m]$ can be replaced by the equivalent one $[nKm]$. We can therefore characterize the bound state by the set of quantum numbers $[n\gamma m]$ where $\gamma=l$ for spherical and $\gamma=K$ for parabolic partial waves. In addition, it must be noted that the projection onto any subspace characterized by a given n must be performed at an appropriate hyper-radius, called R_n [19]. Once the projected wave function $\Psi_{n\gamma m}$ is obtained, it is convenient to define the associated reduced wave function $\Phi_{n\gamma m}$ following Eq. (3) of Ref. [19]. This way indeed, physical quantities take more compact forms, free of both the standard volume element and the semiclassical outgoing wave that describes the bulk of the hyper-radial motion. This reduced wave function reads

$$\Phi_{n\gamma m}(R_n;\alpha,\Omega) = R_n^3 \cos\alpha \sin\alpha\, S_{n\gamma m}(R_n) Y_{1m}(\theta,\varphi) \times \phi_{n\gamma m}(R_n \sin\alpha, \theta_{12}, 0), \quad (3)$$

where we have assumed that the bound electron is electron 2 located at the distance $r_2 = R_n \sin\alpha$ from the origin [26].

The amplitude function $S_{n\gamma m}(R_n)$ and the one-electron bound orbital $\phi_{n\gamma m}(R_n \sin\alpha, \theta_{12}, 0)$ are given in the spherical case by

$$\phi_{nlm}(R_n \sin\alpha, \theta_{12}, 0) = F_{nl}(R_n \sin\alpha) Y_{lm}(\theta_{12}, 0), \quad (4)$$

$$S_{nlm}(R_n) = (-1)^l \{\langle l-m\,1m | l+1\,0\rangle I^-_{nll}(R_n) + \langle l-m\,1m | l-1\,0\rangle I^+_{nll-1}(R_n)\}. \quad (5)$$

The integrals $I^{\pm}_{nlL}(R_n)$ which appear above are defined according to Eq. (37) of Ref. [19] as

$$I^{\pm}_{nlL}(R_n) = \frac{1}{\sqrt{2}} \int_0^{\pi/2} d\alpha \sin\alpha F_{nl}(R_n \sin\alpha) \times [a^+_L(R_n,\alpha) \pm a^-_L(R_n,\alpha)], \quad (6)$$

where the $a^{\pm}_L(R_n,\alpha)$ are the expansion coefficients of the reduced photoabsorption wave function $\Phi(R)$ on the symmetrized and antisymmetrized bipolar harmonics. Their relation to the $f^{\pm}_l(R,\alpha)$ introduced above is easily deduced from Eq. (3) of Ref. [19] which connects the wave functions Ψ and Φ.

Rewriting the spherical amplitudes of Eq. (5) explicitly for the two cases of interest, namely, $m=0$ and $m=\pm 1$, evidences an approximate selection rule in the limit $n,l \to \infty$. Let us then write

$$S_{nl0}(R_n) = \frac{(-1)^l}{\sqrt{2l+1}} \{I^-_{nll}(R_n)\sqrt{l+1} - I^+_{nll-1}(R_n)\sqrt{l}\}, \quad (7)$$

$$S_{nl\pm1}(R_n) = \frac{(-1)^l}{\sqrt{2(2l+1)}} \{I^-_{nll}(R_n)\sqrt{l} + I^+_{nll-1}(R_n)\sqrt{l+1}\}. \quad (8)$$

In the limit $n,l \to \infty$, which is approached only if strong correlations develop into the system, the antisymmetric coefficients a^-_L become negligible with respect to their symmetric counterparts a^+_L in Eq. (6). As a result, $I^+_{nlL} \to I^-_{nlL}$. Considering in addition that $l \pm 1 \to l$ in the limit of large l, we observe that $S_{nl0}(R_n) \to 0$ in this limit. Otherwise stated, $|m|=1$ states are favored. In addition, these states are populated owing to the components of the photoabsorption wave function which are symmetric in the exchange of the radial coordinates of the two electrons $r_1 \leftrightarrow r_2$ or, equivalently, $\alpha \leftrightarrow (\pi/2-\alpha)$. Note that they cannot be characterized as symmetric or antisymmetric by themselves since this property does not make sense at large R for bound and free non overlapping electronic orbitals. Despite this fact, and although this is to some extent a misuse of language, we summarize these observations by stating that the continuum states formed by one free and one bound electron in a highly excited level n satisfy the same approximate selection rules as the series of autoionizing doubly excited states that converges to them, namely, $m=|T|=1$ and $A=+1$. Note, the results relative to a $^3P^o$ photoabsorption wave function can be deduced from the present ones by exchanging the coefficients a^+_L and a^-_L: this leaves the integral I^+_{nlL} unaltered whereas it changes I^-_{nlL} into $-I^-_{nlL}$. As a result, for a $^3P^o$ symmetry, radial correlations favor the $m=T=0$ components in the high n and l limit.

The bound orbitals ϕ_{nKm}, expressed in terms of parabolic coordinates of the bound electron, are given in standard textbooks [9,10]. They are related to their spherical counterparts ϕ_{nlm} by an orthonormal transformation the coefficients of which have been discussed in detail by Hughes [21]:

$$\langle \phi_{nlm} | \phi_{nKm} \rangle = (-1)^{(n-1+K-m)/2} \left\langle \frac{n-1}{2} \frac{m+K}{2} \frac{n-1}{2} \frac{m-K}{2} \middle| lm \right\rangle. \quad (9)$$

It is interesting to note here that $(m \pm K)/2$ and $(n-1)/2$ must be either both integer or both half-integer. Otherwise stated, $n-K$ has the parity of $m-1$. In the present case of a $^1P^o$ symmetry where the only allowed values of m are 0, ± 1, this implies that the parity of $n-K$ determines $|m|$ itself: odd values of $n-K$ imply $m=0$, even values $m=\pm 1$. The approximate $|m|$ selection rule outlined in the preceding paragraph is therefore accompanied, in the case of parabolic states, by a selection rule regarding the parity of K. The orthonormal transformation defined by Eq. (9) also relates the parabolic amplitudes $S_{nK0}(R_n)$ and $S_{nK\pm1}(R_n)$ to their spherical counterparts $S_{nl0}(R_n)$ and $S_{nl\pm1}(R_n)$, so that

$$S_{nK0}(R_n) = \sum_{l=0}^{n-1} (-1)^l \begin{pmatrix} \frac{n-1}{2} & \frac{n-1}{2} & l \\ \frac{K}{2} & -\frac{K}{2} & 0 \end{pmatrix} \{I^-_{nll}(R_n)\sqrt{l+1} - I^+_{nll-1}(R_n)\sqrt{l}\}, \quad (10)$$

$$S_{nK1}(R_n) = \frac{1}{\sqrt{2}} \sum_{l=1}^{n-1} (-1)^l \begin{pmatrix} \frac{n-1}{2} & \frac{n-1}{2} & l \\ \frac{1+K}{2} & \frac{1-K}{2} & -1 \end{pmatrix} \{I^-_{nll}(R_n)\sqrt{l} + I^+_{nll-1}(R_n)\sqrt{l+1}\}, \quad (11)$$

and $S_{nK-1} = -S_{nK1}$, where we have rewritten Clebsch Gordan coefficients in terms of $3j$ coefficients for convenience.

C. Partial ionization-excitation cross sections

The partial integrated and differential cross sections are obtained from the flux of $\Psi_{n\gamma m}$ through an hypersurface of radius R_n. They can be expressed very simply from the reduced wave function $\phi_{n\gamma m}$. The integrated cross section, for instance, is given according to Eq. (29) of Ref. [19] by

$$\sigma_{n\gamma m} = 2\frac{2\pi\omega}{c} \int_{R=R_n} d\alpha d\Omega |\Phi_{n\gamma m}(R,\alpha,\Omega)|^2. \quad (12)$$

A straightforward calculation then yields

$$\sigma_{n\gamma m} = 2\frac{2\pi\omega}{c} R_n^3 |S_{n\gamma m}(R_n)|^2. \quad (13)$$

As to the partial differential cross sections, they can be reconstructed from the above partial integrated cross sections

and the corresponding asymmetry parameters

$$\beta_{n\gamma 0} = +2, \quad \beta_{n\gamma\pm 1} = -1, \tag{14}$$

leading to the very simple expressions below, namely,

$$\frac{d\sigma_{n\gamma 0}}{d\Omega} = \frac{3}{4\pi}\sigma_{n\gamma 0}\cos^2\theta, \tag{15}$$

$$\frac{d\sigma_{n\gamma\pm 1}}{d\Omega} = \frac{3}{8\pi}\sigma_{n\gamma\pm 1}\sin^2\theta. \tag{16}$$

D. Total ionization excitation cross sections

The next step implies that one sums the cross sections over the magnetic quantum number m for a given γ. In the case of parabolic partial waves, due to the one to one correspondence between K and $|m|$ values already outlined, this summation reduces to the $m=0$ term for odd values of $n-K$, and to twice the $m=1$ term for even values. In the case of spherical partial waves, by contrast, the $m=0, \pm 1$ contributions must be added effectively for $l>0$ so that Eqs. (13) and (14) must be completed by

$$\sigma_{nl} = \sigma_{nl0} + 2\sigma_{nl1}, \quad \beta_{nl} = 2\frac{\sigma_{nl0} - \sigma_{nl1}}{\sigma_{nl0} + 2\sigma_{nl1}}. \tag{17}$$

A straightforward calculation then yields simple expressions of these quantities in terms of the elementary integrals $I^{\pm}_{nlL}$ computed at R_n:

$$\sigma_{nl} = 2\frac{2\pi\omega}{c}R_n^3(|I^+_{nll-1}|^2 + |I^-_{nll}|^2), \tag{18}$$

$$\beta_{nl} = \frac{(l+2)|I^-_{nll}|^2 - 6\sqrt{l(l+1)}\,\mathrm{Re}(I^-_{nll}I^{+*}_{nll-1}) + (l-1)|I^+_{nll-1}|^2}{(2l+1)(|I^-_{nll}|^2 + |I^+_{nll-1}|^2)}. \tag{19}$$

The last step then consists in reconstructing the total integrated cross section and asymmetry parameter for a given level n from the contributions of the different partial waves γ. To this end, we introduce

$$\sigma_n^{T=0} = \sum_{l=0}^{n-1}\sigma_{nl0} = \sum_{\substack{K=-n+1 \\ (n-K)\text{odd}}}^{n-1}\sigma_{nK0}, \tag{20}$$

$$\sigma_n^{T=1} = 2\sum_{l=1}^{n-1}\sigma_{nl1} = 2\sum_{\substack{K=-n+2 \\ (n-K)\text{even}}}^{n-2}\sigma_{nK1}, \tag{21}$$

thus obtaining

$$\sigma_n = \sigma_n^{T=0} + \sigma_n^{T=1}, \quad \beta_n = 2\frac{\sigma_n^{T=0}}{\sigma_n} - \frac{\sigma_n^{T=1}}{\sigma_n}. \tag{22}$$

We are now in a position to present and comment our numerical results.

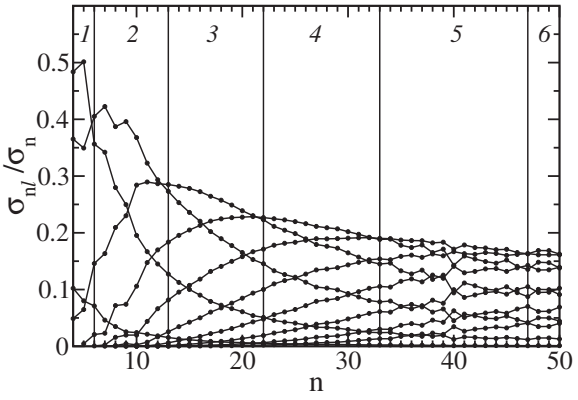

FIG. 1. The relative partial cross sections σ_{nl}/σ_n with respect to n for $l=0$ to 9. Each vertical stripe defines a range of values of n in which the dominant contribution σ_{nl}/σ_n occurs for the same value of l, which is given by the number at the top of the stripe. σ_{n0}/σ_n is the only contribution that decreases monotonously with increasing n.

III. NUMERICAL RESULTS

A. Spherical partial waves

Figure 1 shows the relative partial cross sections σ_{nl}/σ_n plotted with respect to n for the first ten l partial waves. From these fixed-l n distributions, the dominant l_{dom} can be roughly estimated: $l_{\mathrm{dom}}=1$ for $4<n\leqslant 5$, $l_{\mathrm{dom}}=2$ for $6\leqslant n\leqslant 12$, $l_{\mathrm{dom}}=3$ for $13\leqslant n\leqslant 21$, $l_{\mathrm{dom}}=4$ for $22\leqslant n\leqslant 32$, $l_{\mathrm{dom}}=5$ for $33\leqslant n\leqslant 46$, and $l_{\mathrm{dom}}=6$ for $47\leqslant n\leqslant 50$. These general trends are compatible with Greene's results presented in Fig. 6 of Ref. [22]: the latter shows an l distribution that has two main components $l=1$ and 2, for $n=4$, the second one, $l=2$, becoming dominant for $n=6$. The present Fig. 1 evidences the mixing of l values, which becomes more and more pronounced as n increases: at $n=10$, the accumulated four most important l contributions reach 95% of the total cross section. This proportion drops down to 60% at $n=50$. In other words, l is definitively not a good quantum number, all the worst the higher n.

The fixed-n l distributions shown on Fig. 2 carry the same observations: as n increases, the l distribution shifts towards higher l, flattens, and widens. This evolution seems, however, to slow down between $n=40$ and $n=50$ as the corresponding thick dashed-dotted and continuous lines can hardly be distinguished. For each n, an ansatz of the form $a_0(2l+1)\exp\left[-\left(\frac{l-a_1}{a_2}\right)^2\right]$ has been fitted to the l distribution, thus providing a noninteger mock-dominant angular momentum $l_{\mathrm{dom}}(n)$, the evolution of which is displayed on Fig. 3. Two trial functions have been fitted to the observed $l_{\mathrm{dom}}(n)$: the three-parameter formula $a_0+a_1n^{a_2}$ and the two-parameter formula $a_0+a_1n^{0.5}$ yield equal-quality fits which cannot be distinguished at the scale of the figure. The trial laws obtained are $-0.999+1.10n^{0.456}$ and $-0.626+0.88n^{0.5}$. It can be noticed that the first law is close to $2\tilde{l}^R_{\mathrm{dom}}$, while the second one can be written $1.24\tilde{l}^D_{\mathrm{dom}}$. However, none of these two laws is in perfect agreement either with l^D_{dom} or l^R_{dom} or with $\tilde{l}^D_{\mathrm{dom}}$ or $\tilde{l}^R_{\mathrm{dom}}$. This will be understood easily from the parabolic

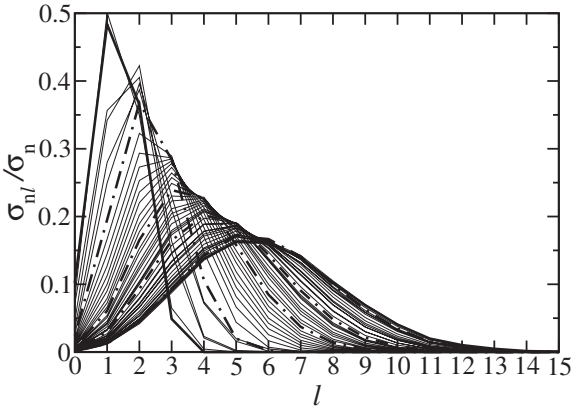

FIG. 2. Relative partial cross sections σ_{nl}/σ_n with respect to l for $n=4$ to 50. The first $n=4$ and last $n=50$ distributions are emphasized by thick full lines, the intermediate $n=10,20,30,40$ by thick dashed-dotted ones

partial wave analysis below. For the time being, we just point out that the $\sqrt{n}$ behavior of l_{dom} is confirmed by our calculations to a reasonable extent.

B. Parabolic partial waves

Figure 4 shows the relative parabolic cross sections σ_{nK}/σ_n as a function of $n-K$ for a sample of n values. It evidences approximate selection rules. First of all, "favored" $(n-K)$ even $|m|=T=1$ states alternate with "unfavored" $(n-K)$ odd $|m|=T=0$ ones. Second, the signal decreases very quickly as $(n-K)$ increases, cancelling down to zero long before $(n-K)$ reaches its maximum allowed value $2n-1$. In other words, the process is dominated by a few values of K, namely, the largest ones having the parity of n, that is to say $n-2$, $n-4$, $n-6,\ldots$.

Figure 5 offers more insight into the relative weights of the various K partial waves. It displays the relative parabolic partial cross sections σ_{nK}/σ_n as a function of n for the first few relevant values of K. Even $(n-K)$ partial waves are represented on the left plot, odd $(n-K)$ ones on the right plot. The obviously different scales of the two plots outline the dominant character of the "favored" $|m|=T=1$ states. In addition, both pictures display the singular behavior of the largest K partial wave in each class of states, the contribution of which is largely dominant at small n, but less and less so with increasing n, as the mixing with smaller values of K becomes more important. This mixing remains, however, much less pronounced than in the spherical representation: at $n=10$, the accumulated four most important contributions reach 93% of the total cross section, a proportion that drops down only slowly with increasing n, as it still amounts to 80% at $n=50$. Another difference with respect to the spherical case is that there are no curve crossings on either plots of Fig. 5. Compared to l, K is therefore a much better candidate to apply as an approximate good quantum number.

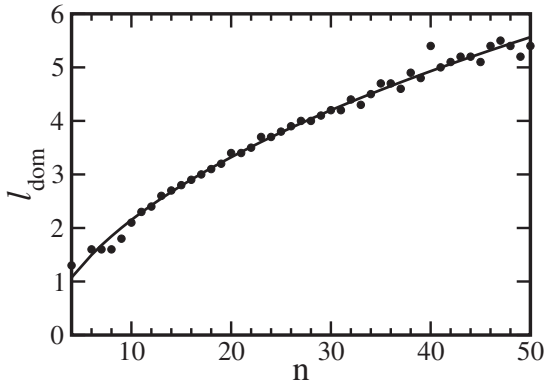

FIG. 3. Noninteger mock-dominant angular momentum l_{dom} with respect to n.

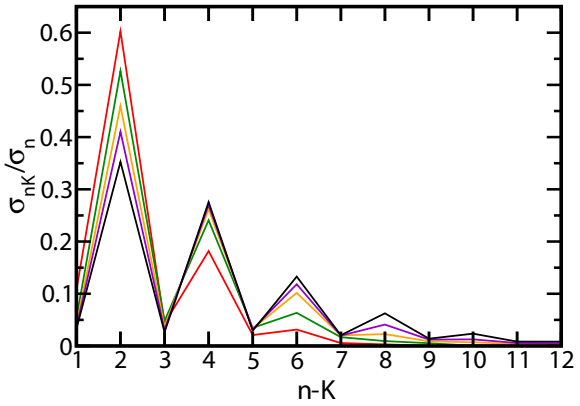

FIG. 4. (Color online) Relative parabolic cross sections σ_{nK}/σ_n with respect to $n-K$ for $n=10$ (red), 20 (green), 30 (orange), 40 (violet), and 50 (black).

Thus, in contrast to spherical partial cross sections, parabolic partial cross sections obey approximate selection rules: namely, ionization excitation to the level n proceeds mainly through $T=1$ and $K=n-2$. This approximate goodness of the (K,T) quantum numbers originates in their relation to electronic correlations. The rapid extinction of the $|m|=T=0$ contribution, which drops below 10% for $n>10$, has been anticipated: we have already noted above that the $|m|=T=0$ amplitude of Eq. (7) should be suppressed in the limit of high n and l due to the domination of the radially symmetric components of the photoabsorption wave function in this limit. This extinction is therefore the signature of the radial correlations. On the other side,

$$\langle \phi_{nKm}|\cos\theta_{12}|\phi_{nK'm'}\rangle = -\frac{K}{n}\delta_{KK'}\delta_{mm'}, \tag{23}$$

shows that within a given n subspace, the larger K, the closer the two electrons to the back to back configuration $\theta_{12}=\pi$. The domination of large positive values of K is therefore the signature of angular correlations.

In addition, as announced in the preceding paragraph, these results make clear why Drukarev's [3] and Rau's [4] models cannot yield quantitative estimates of the dominant spherical partial wave l_{dom}. These authors indeed assume that the system is in the state of "maximum asymmetry," meaning that the electrons are as close as possible to the antiparallel configuration $\hat{r}_1=-\hat{r}_2$. This state is described by $n_2=n-1$,

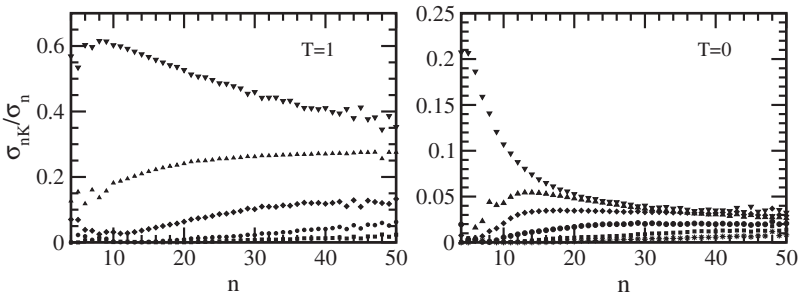

FIG. 5. Relative parabolic cross sections σ_{nK}/σ_n with respect to n. Left plot $T=1$ contributions. Down triangles: $K=n-2$; up triangles: $K=n-4$; diamonds: $K=n-6$; circles: $K=n-8$; squares: $K=n-10$. Right plot $T=0$ contributions. Down triangles: $K=n-1$; up triangles: $K=n-3$; diamonds: $K=n-5$; circles: $K=n-7$; squares: $K=n-9$; stars: $K=n-11$.

$n_1=0$ in the parabolic approach and by $K=n-1$, $T=0$ in the group theoretical approach. For a $^1P^o$ symmetry however, this $T=0$ state is unfavored, so that one cannot expect these treatments to apply quantitatively in this case. More importantly, in their derivation, these authors assume $n \gg 1$: for large n, however, the mixing of K values becomes nonnegligible, so that their hypothesis of a single contributing K value fails.

C. Relation of ionization-excitation to double ionization and double excitation

This analysis provides deeper insight into the relation between ionization excitation and the related processes of double ionization and double excitation. Radially symmetric back to back configurations $\vec{r}_1=-\vec{r}_2$ of the two electrons were indeed shown by Wannier [1] to play a dominant role in the dynamics of double escape. In the present case of a $^1P^o$ two electron wave function, however, the existence of a conflict between angular and radial correlations adds some complexity to the original Wannier picture. This conflict is usually described in terms of opposite requirements of the parity $\Psi(-\vec{r}_1,-\vec{r}_2)=-\Psi(\vec{r}_1,\vec{r}_2)$ and spin $\Psi(\vec{r}_2,\vec{r}_1)=\Psi(\vec{r}_1,\vec{r}_2)$ in the Wannier configuration $(\vec{r}_1=-\vec{r}_2)$, leading to a paradoxical node of the wave function in this "favored" geometry [23]. In the language of parabolic quantum numbers, it shows through the fact that the state of maximum $K=n-1$ selected by the angular correlations is forbidden by the radial correlations, owing to its $|m|=T=0$ character. With this reserve, the present study, which enlightens the dominant contribution of the $K=n-2$, $T=1$, $A=+1$ parabolic partial ionization-excitation cross sections, confirms the importance of the Wannier configuration in the low-energy two-electron dynamics whatever the outgoing channel considered, be it double ionization or ionization excitation, as anticipated by Fano [2].

On the other side, the works of Herrick and coworkers [11–15], Feagin and Briggs [16], and Lin [17,18] have led to characterize the members $n' \geqslant n$ of Rydberg series of doubly excited states of $^{2S+1}L^{\pi}$ symmetry converging toward the nth ionization threshold of He by the additional quantum numbers K, T, and A. The photoabsorption spectrum of He below the nth ionization threshold was then found experimentally to be dominated by $[_{n'}(KT)^A_n;{}^1P^o]$ states with $K=n-2$, $T=1$, $A=+1$, and $n' \geqslant n$. The present study shows that the continuum states populated by ionization excitation obey the same selection rules as the abovementioned doubly excited states: therefore, they appear as the limits of the $[_{n'}(KT)^A_n;{}^1P^o]$ series for $n' \to \infty$.

D. Asymmetry parameter for ionization excitation: Asymptotic limit, relation to electronic correlations

At this point, it is worth paying a little bit more attention to the asymmetry parameter β_n. First of all, as the T selection rule enforces itself very rapidly with increasing n, the relative contributions $\sigma_n^{T=0}/\sigma_n$ and $\sigma_n^{T=1}/\sigma_n$ reach their asymptotic limits very quickly: the asymptotic limit of β_n can then be obtained from Eq. (22). The procedure is illustrated in Fig. 6 which shows $\sigma_n^{T=0}/\sigma_n$, $\sigma_n^{T=1}/\sigma_n$, and β_n as a function of n. An expression of the form $a_0+a_1 n^{-1/2}$ has been fitted to each of these quantities independently. The resulting expressions of $\sigma_n^{T=0}/\sigma_n$ and $\sigma_n^{T=1}/\sigma_n$ add to 1 as expected. Moreover, their linear combination defined by Eq. (22) is identical to the expression resulting from a direct fit to β_n. This cross checking gives us confidence into these fitted formulas. Accordingly, we believe that the corresponding asymptotic value of β_n, namely, $\beta_\infty=-0.71$, is more reliable than the value of -0.636 we derived in Ref. [19].

In addition, one should note that the observed value of β_n results from the interplay of symmetry requirements and radial correlations. In the present case of a $^1P^o$ wave function, radial correlations strongly favor the $|m|=T=1$ components, as discussed above. As these components are associated to the value -1 of the asymmetry parameter, the resulting β_n clearly tends towards -1 for large n. In the complementary case of a $^3P^o$ wave function, radial correlations would favor

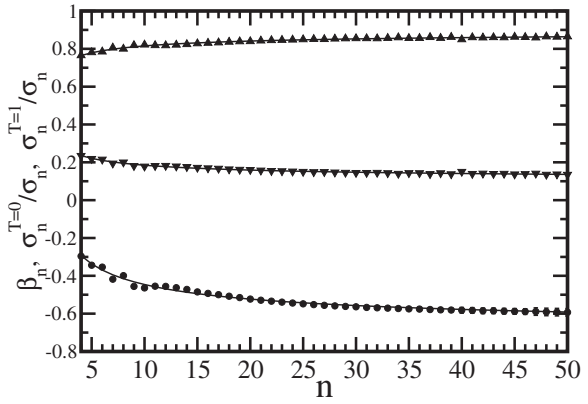

FIG. 6. Determining the limit of β_n as $n \to \infty$. From bottom to top. Circles: β_n; down triangles: $\sigma_n^{T=0}/\sigma_n$; up triangles: $\sigma_n^{T=1}/\sigma_n$. Continuous lines: fits (see text).

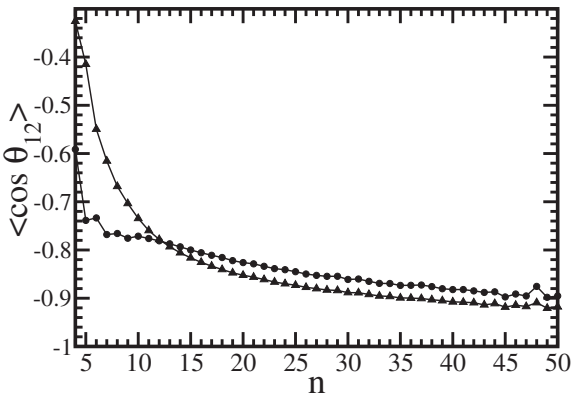

FIG. 7. Mean value of $\cos\theta_{12}$. Circles: in $(n,T=0)$ subspace; up triangles: in $(n,T=1)$ subspace.

the $|m|=T=0$ components associated to $\beta=+2$, and the resulting β_n would tend towards +2 for large n in agreement with former predictions by Greene [20]. This leads us to suspect that, contrary to widespread belief, the asymmetry parameter has little to do with angular correlations. The calculation of the average value of $\cos\theta_{12}$ in the subspaces $(n,T=0)$ and $(n,T=1)$ provides further support to this statement. The two curves of Fig. 7 indeed show a similar evolution: they decrease monotonously with n, rapidly till $n \simeq 10$ and then more slowly, to finally tend towards -1 at large n. This demonstrates that angular correlations, which favor the back to back configuration of the two electrons, express themselves equally well within the $T=0$ and $T=1$ subspaces, despite the fact that these two subspaces lead to quite opposite values of the asymmetry parameter, namely, +2 for the former and -1 for the latter. In other words, angular correlations influence the relative arrangement of the three body system, they do not affect its absolute orientation with respect to the polarization vector of the incident light. Note also that the evolution pattern of $\cos\theta_{12}$ with n is consistent with a θ_{12} distribution centered at $\theta_{12}=\pi$, the width of which decreases as n increases, whereas the number of contributing spherical partial waves increases as shown by Fig. 2.

IV. CONCLUSION

The above analysis of photoionization excitation shows that the parabolic partial cross sections σ_{nK} are much more selective with respect to K than the spherical partial cross sections σ_{nl} with respect to l. Moreover, the asymmetry parameter β_{nK} takes the known values +2[−1] for odd [even] values of $n-K$, whereas the value of β_{nl} results from the detailed coupling of neighboring partial waves l, $l\pm1$. This means that the integrated partial cross section σ_{nK} can be deduced from the measurement of the differential partial cross section $d\sigma_{nK}/d\Omega$ at a unique angle. Generally speaking, parabolic partial cross sections give more direct insight than spherical partial cross sections into the correlated two-electron dynamics. Above the double ionization threshold, the relative weights of the σ_{nK} for the various values of K mimic the relative importance of the corresponding Rydberg series of doubly excited states $(KT)^A_n$ converging toward the nth ionization threshold. Below the double ionization threshold, autoionization to the nK Stark level of the residual He^+ ion is the preferred decay channel of doubly excited states belonging to the series $[(K+1)T]^A_{n'>n}$, according to the propensity rules proposed by Rost and co-workers [24]. All these properties make it very desirable to measure parabolic partial cross sections defined with respect to the photoelectron direction. The most obvious strategy would consist in applying a static electric field over the interaction region and energy analyzing the photoelectrons emitted along this field. However, the field needed to induce some 10 meV splitting of the Stark levels of the residual ion would accelerate the emitted photo electrons by some tens of kV making it impossible to analyze them with a sufficient energy—if not angular—resolution. The measurement of parabolic partial cross sections therefore appears as a challenge to experimentalists.

ACKNOWLEDGMENTS

We acknowledge the support of the CNRS computer center IDRIS (Orsay, France) through Project No. 061485.

[1] G. H. Wannier, Phys. Rev. **90**, 817 (1953).
[2] U. Fano, J. Phys. B **7**, L401 (1974).
[3] G. F. Drukarev, Zh. Eksp. Teor. Fiz. **83**, 946 (1982); Sov. Phys. JETP **56**, 532 (1983).
[4] A. R. P. Rau, J. Phys. B **17**, L75 (1984).
[5] P. Hammond, F. H. Read, and G. C. King, J. Phys. B **21**, 3123 (1988).
[6] P. R. Woodruff and J. A. R. Samson, Phys. Rev. A **25**, 848 (1982).
[7] J. R. Harries, J. P. Sullivan, S. Obara, P. Hammond, and Y. Azuma, J. Phys. B **36**, L319 (2003).
[8] J. R. Harries, J. P. Sullivan, S. Obara, Y. Azuma, J. G. Lambourne, F. Penent, R. I. Hall, P. Lablanquie, K. Bucar, M. Zitnik, and P. Hammond, J. Phys. B **38**, L153 (2005).
[9] H. A. Bethe and E. E. Salpeter, *Quantum Mechanics of One- and Two-Electron Atoms* (Academic, New York, 1957).
[10] L. D. Landau, E. M. Lifshitz, J. B. Sykes, and J. S. Bell, *Quantum Mechanics. Non-relativistic Theory* (Pergamon, Oxford, 1965).
[11] O. Sinagoglu and D. R. Herrick, J. Chem. Phys. **62**, 886 (1973).
[12] D. R. Herrick and A. O. Sinanoglu, Phys. Rev. A **11**, 97 (1975).
[13] D. R. Herrick and M. E. Kellman, Phys. Rev. A **21**, 418 (1980).
[14] D. R. Herrick, M. E. Kellman, and R. D. Poliak, Phys. Rev. A **22**, 1517 (1980).
[15] M. E. Kellman and D. R. Herrick, Phys. Rev. A **22**, 1536

(1980).
[16] J. M. Feagin and J. S. Briggs, Phys. Rev. A **37**, 4599 (1988).
[17] C. D. Lin, Phys. Rev. Lett. **51**, 1348 (1983).
[18] C. D. Lin, Phys. Rev. A **29**, 1019 (1984).
[19] C. Bouri, P. Selles, L. Malegat, J. M. Teuler, M. Kwato Njock, and A. K. Kazansky, Phys. Rev. A **72**, 042716 (2005).
[20] C. H. Greene, Phys. Rev. Lett. **44**, 869 (1980).
[21] J. W. B. Hughes, Proc. Phys. Soc. London **91**, 810 (1967).
[22] P. A. Heimann, U. Becker, H. G. Kerkhoff, B. Langer, D. Szostak, R. Wehlitz, D. W. Lindle, T. A. Ferrett, and D. A. Shirley, Phys. Rev. A **34**, 3782 (1986).
[23] A. D. Stauffer, Phys. Lett. **91A**, 114 (1982).
[24] J. M. Rost *et al.*, J. Phys. B **30**, 4663 (1997).
[25] To be precise, the function we consider here is obtained by subtracting the ionization-excitation channels $n=1,2,3$ from the full photoabsorption wave function $\bar{\Psi}(\vec{r}_1,\vec{r}_2)$ defined in Ref. [19]: see Eqs. (1) and (3) and the beginning of Sec. II C for more detail.
[26] Changing α into $(\pi/2-\alpha)$ yields the result for the opposite situation in which electron 2 is the photoelectron.